Scandinavian Symposium on Physical Acoustics, Geilo, Jan 29th - Feb 1st, 2012

Sound velocity change owing to the acousto-elastic/plastic effect in steel measured using Acoustic Resonance Technology (ART)

Simen Eldevik *
Det Norske Veritas [1]

Åge A. F. Olsen
Det Norske Veritas [1]

Per Lunde
University of Bergen [2]

Abstract

Non-destructive stress measurement of structures is increasingly valued by the industry. Ultrasonic methods have the advantage that acoustic waves propagate with ease through materials, making it possible to probe the interior of structures. This paper investigates the possibility of utilising the acousto-elastic/plastic effect, where the sound velocity of a medium is dependent on the applied stress state, together with an ultrasonic technique based on transient acoustic reflections called Acoustic Resonance Technology (ART), to measure the dependency between sound velocity and induced stress state during tension testing. A measured relative velocity change in the order of a few tenths of one percent has been observed. The presented results have been based on only one set of test specimens and further work is needed to consolidate and quantify the variation of the dependency.

Keywords: acousto-elasticity, acousto-plasticity, stress, strain, resonance, sound velocity

1 Introduction

As the industry strives to reduce maintenance and repair costs, non-destructive testing of structures becomes increasingly valued both in production control and as a means to measure the utilisation and condition of key infrastructure. There are several non-destructive testing (NDT) techniques which measure stress [1] - [3]. Techniques using optical measurements, magnetic measurements, x-ray diffraction, or the deeper penetrating ($<$50 mm) neutron diffraction are all limited to measuring surface or near surface stress or strains. However, for structural integrity the stress/strain state in the interior of the medium is important. Acoustic waves propagate with ease through materials and thus provide a means to probe the interior of structures.

The acousto-elastic effect [4, 5] describes how the velocity of sound changes subtly in an elastically deformed body. The effect has been studied in several experiments and modelled by different researchers [6] - [11]. In particular, for bi-axially loaded samples the longitudinal sound velocity (c_l) increases with applied load while the shear velocities (c_s) polarised parallel and perpendicular to the load decrease. This is already exploited in some NDE applications, in which bi-static transducer setups are used to measure time-of-flight over relatively small ranges [12].

Knowledge of the failure modes of materials and structures have led to many structures being allowed to plastically deform within some limitations. As the material starts to plastically deform, it is altered on a molecular scale as grain boundaries and dislocations move in response to the applied load, and the elastic description is no longer valid [13]. This will affect the acoustic properties of the material, and the effect has been called the acousto-plastic effect [14, 15]. Some experimental work focusing on the NDT application of the acousto-plastic effect was reported in [11], [16] - [18].

*simen.eldevik@dnv.com
[1]Det Norske Veritas, Veritasveien 1, NO-1322 Høvik, Norway
[2]University of Bergen, Department of Physics and Technology, Allegt. 55, NO-5020 Bergen, Norway

This paper describes an experimental setup utilising an acoustic resonance frequency technique to measure the change in sound velocity of steel with increasing strain in the acousto-elastic and acousto-plastic region. The focused here is on the change of the longitudinal sound velocity in steel with increasing strain. However, the method described can potentially be used to measure changes in both the longitudinal and shear sound velocities.

2 Experimental setup

The Acoustic Resonance Technology (ART) methodology developed by Det Norske Veritas (DNV) is based on transient acoustic reflections from layers and plates [19, 20]. A broad band signal impinging on a plate will be reflected from both the front and back interface of the plate. For the frequencies where an integer multiple of the half wave length $\lambda/2$ matches the thickness of the plate d the plate response will be resonant (i.e. where $d = n\lambda/2, n = 1, 2, 3, \ldots$). The transmitted signal is thus reflected as a main echo followed by a lower amplitude tail which mainly consists of the half-wave resonance frequencies. For a given sound velocity c (e.g. c_l or c_s) the frequency is given by the relation $f = c/\lambda$. Thus for thickness extensional (TE) modes and thickness shear (TS) modes based on the longitudinal and shear velocities, respectively, the resonance frequencies are given by:

$$f_n^{l/s} = \frac{nc_{l/s}}{2d}, \qquad n = 1, 2, 3, \ldots \tag{1}$$

where subscript n denotes the harmonic number, l/s denotes longitudinal or shear velocity. Based on the measured resonance frequency and the thickness of the sample it is thus possible to calculate the average sound velocity across the test specimen. The relative sound velocity change is then given by:

$$c_r = \frac{c}{c_0} = \frac{df_n}{d_0 f_{n0}} \tag{2}$$

where subscript 0 denotes the reference values measured at the start of the test (i.e. at zero loading).

The test specimens used in this experiment were rectangularly shaped S355J2 [21] steel samples of thickness 10 mm, width 50 mm, and length 600 mm. The coordinate system was oriented with the length, width, and thickness dimensions in the x-, y-, and z-directions, respectively. A sketch of the specimens and the coordinate system are shown in Fig. 1. On the two long sides U-shaped notches were

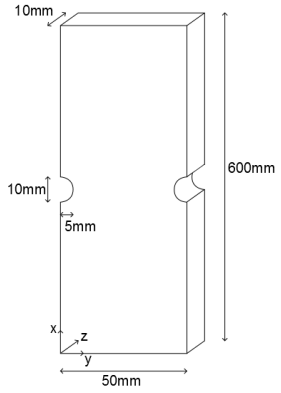

Figure 1: Rectangular specimen with a U-notch to locate plastic deformation

machined to localise the plastic deformation. Based on a specimen thickness of 10 mm and the typical longitudinal and shear sound velocities in steel of 6000 m/s and 3300 m/s respectively, Eq. (1) gives the expected nominal resonance frequencies given in Table 1.

Table 1: Longitudinal and shear harmonic frequencies

n	**Thickness extensional modes** f_n^l (kHz)	**Thickness shear modes** f_n^s (kHz)
1	300	165
2	600	330
3	900	495

The ART transducer was aligned in such a way that the acoustic footprint was centered between the two notches shown in Fig. 1, measuring the fundamental half-wave resonance frequency and its overtones across the thickness of the test specimen (z-direction) during loading.

The distance between the ART transducer and the specimen was approximately 11 cm, and the acoustic footprint on the specimen of the order of 2 cm. A box model and schematic of the setup is shown in Fig. 2. A 30 μs chirp signal with frequencies spanning from 100 kHz to 1 MHz was generated and transmitted by a custom built near field transducer (i.e. the specimen under investigation is placed within the near-field limit of the transducer) produced by PCT Ltd [22] with a relatively flat operating frequency band from 300 kHz to 800 kHz.

To get a statistical distribution of resonance frequencies for different loading, the ART system was set up to do sequences of 50 acoustic shots with a latency of approximately 10 s between each group of shots. Each group of 50 measurements has thus a distribution of resonance frequencies for a small variation in applied displacement and force. The load history is shown in Fig. 4 and is discussed in Sec. 4.

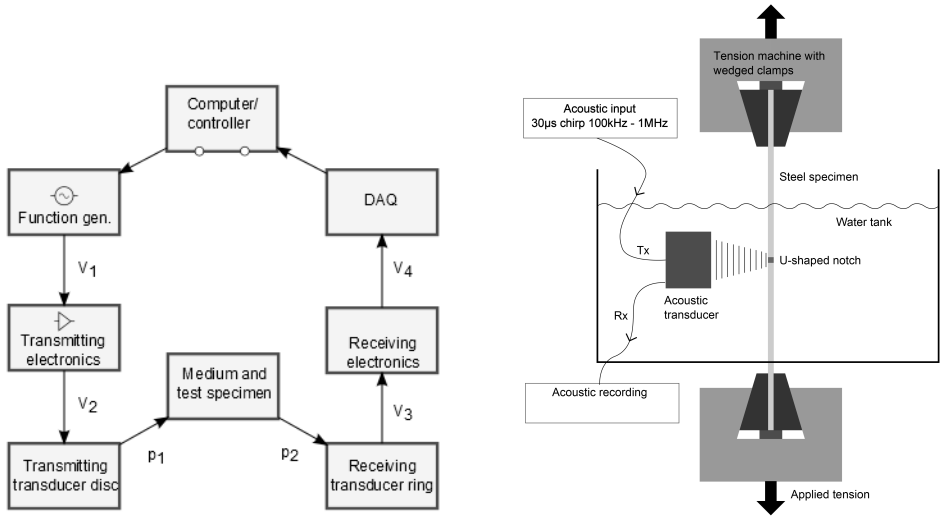

(a) ART box model (b) Tension machine and ART set-up (side view)

Figure 2: ART measurement set-up

The ART system was set up inside a water tank which was fitted to an Instron 8502 [23] tension machine, with a load capacity of 300 kN in tension. The test specimen was inserted through a sealed hole in the bottom of the water tank and into the loading cell, where it was fixed using two sets of wedged clamps with a clamping pressure of approximately 550 bar and a serrated clamping face. A sketch of the tension machine is shown in Fig. 2b. A control unit from MessTek [24] were used to control the applied load during the tests. The load history used in the experiment consisted of four displacement controlled loading sequences with a displacement velocity of 1.5 mm/s, with subsequent force controlled unloading with an unloading velocity of 100 kN/s.

The mechanical tension was changed continuously during loading and unloading to reduce the effect of fluctuations in force and displacement owing to the integral control system of the tension machine. Each

acoustic measurement had a duration of approximately 500 ms, which corresponds to a displacement in the order of 15 μm or a load in the order of 0.8 kN for the displacement/force controlled loading.

Since the specimens were subjected to destructive loading during the tests, each specimen could only be used once.

As the load was applied in the x-directon (see Fig. 1) the Poisson effect reduces the thickness of the sample. From Eq. (1) it is clear that a negative relative change in thickness will have the same effect on the measured frequency as a corresponding positive relative change in sound velocity. Thus, to be able to separate the contribution owing to thickness change and the contribution owing to change in sound velocity for the measured resonance frequency, independent measurements of the sample thickness is needed. Two systems have been used to this purpose. One is a photometric measurement system called ARAMIS [25, 26] which uses two digital cameras to obtain a stereo image of a stochastic pattern sprayed on the surface of the test specimen. These stereo images can then be used to calculate displacement and strain fields for the imaged area with an accuracy up to 0.01 % strain [27]. A sketch of the ARAMIS measuring system and a resulting strain distribution is shown in figs. 3a and 3b. The 2D strain field

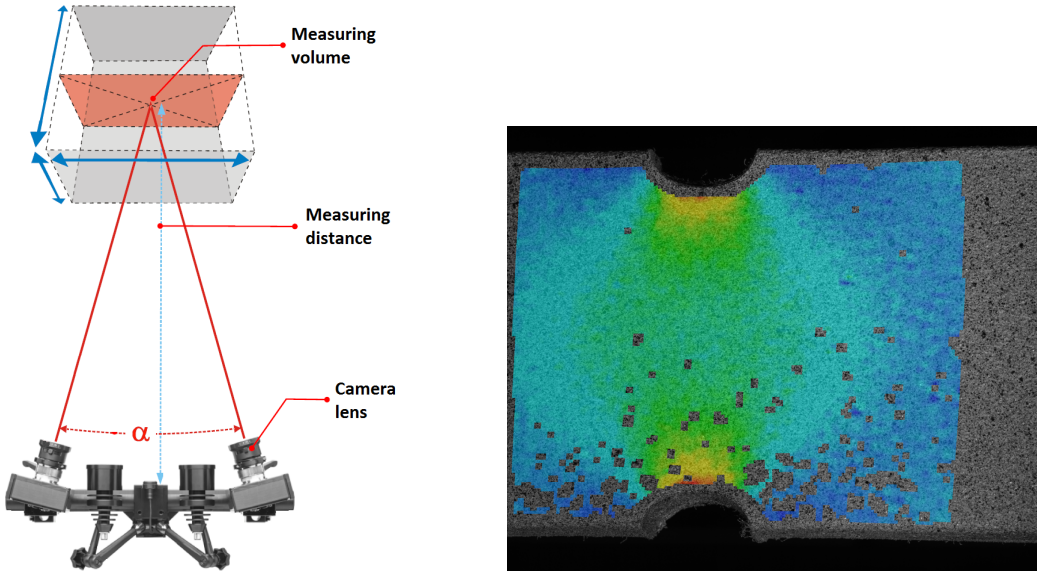

(a) ARAMIS schematic [26]

(b) Strain field

Figure 3: ARAMIS system with example of stochastic pattern and calculated strain field

(i.e. $\varepsilon_x = \Delta x/x$ and $\varepsilon_y = \Delta y/y$) measured by ARAMIS on the surface of the specimen can be used to calculate a thickness reduction strain ($\varepsilon_z = \Delta z/z$), under the assumption of material volume constancy [25]. This gives results distributed over a region of the specimen. The other system consists of two facing needles which are spring loaded to ensure contact with the test specimen. The movement of the needles is measured by an inductive coil and, by calibrating the gap between them, the change in specimen thickness (Δz) can be measured for a point location. The resolution of the needle measuring system is 2 μm. The needle measurements were used to corroborate the ARAMIS measurements.

A challenge in the current setup is that the acoustic response and the geometric deformation can not be measured simultaneously. To overcome this, 2 sets of experiments were performed; one set for acoustic measurements and one set for geometric measurements. Unfortunately, variations in material properties and geometry among the specimens can thus lead to differences in the calculated sound velocities.

3 Measurement uncertainty

The measurement uncertainty comprises the uncertainty of the acoustic measurement, the uncertainty of the thickness measurement, and the statistical variation in material and deformation pattern of the specimens. The latter two have been shown to be the largest and dominant uncertainty (see Table 3).

The linearised approximation of relative standard uncertainty of uncorrelated uncertainty contributions can be expressed as

$$E_z = \frac{u(z)}{|z|} \approx \frac{1}{|z|}\sqrt{\sum_{i=1}^{N}\left(\frac{\partial z}{\partial x_i}\right)^2 u^2(x_i)} \tag{3}$$

where z is a variable or some function of N variables. x_i and $u(x_i)$ is the standard uncertainty of each variable x_i.

The actual variation in material and deformation pattern can be hard to quantify. It consists of the variability in the initial geometry, variation in material properties between specimens, and within each specimen. It depends on how the specimen is inserted in the tension machine and also on the variation in initial thickness and how this is distributed over the specimen. To estimate the order of magnitude of this complex uncertainty, the variation in overall thinning of the specimens has been assumed to be representative. The thickness change has been measured for five specimens, three using ARAMIS and two using the needle setup. These tests resulted in a mean relative thickness change of -6 % and the preliminary relative standard uncertainty (E_{misc}) of ∼7 %, where *misc* denotes these miscellaneous uncertainty contributions.

The thickness measurement is a combination of a micrometer screw measurement of the undeformed thickness and a relative thickness change measurement (ARAMIS) or an absolute thickness change measurement (needle):

$$d = d_0(1+\varepsilon_d) \tag{4}$$

$$d = d_0 + \Delta d \tag{5}$$

where subscript 0 denotes the undeformed thickness measured with a micrometer screw and ε_d and Δd denotes thickness change measurement by ARAMIS and needle, respectively. Although only ARAMIS measurements have been used in this paper, the uncertainty analysis for the needle measurements is included for reference. Eqs. (2) and (4) leads to the relationship for the ARAMIS measurements

$$c_r = \frac{c_l}{c_{l0}} = \frac{(1+\varepsilon_d)f_n}{f_{n0}} \tag{6}$$

where f_n and f_{n0} is the measured frequency and the reference frequency respectively, and ε_d is the thickness strain. For the needle measurements Eqs. (2) and (5) yields the relationship

$$c_r = \frac{c_l}{c_{l0}} = \frac{(d_0+\Delta d)f_n}{t_0 f_{n0}} = \left(\frac{\Delta d}{d_0}+1\right)\frac{f_n}{f_{n0}} \tag{7}$$

where the thickness change Δd is the measured difference between the reference thickness d_0 and the current thickness d. This leads to the uncertainty relation for the ARAMIS $^{(a)}$ measurements

$$\begin{aligned} E_{c_r}^{(a)} &= \frac{u(c_r)}{c_r}^{(a)} \\ &\approx \sqrt{\left(\frac{\varepsilon_d}{1+\varepsilon_d}\right)^2\left(\frac{u(\varepsilon_d)}{\varepsilon_d}\right)^2 + \left(\frac{u(f_n)}{f_n}\right)^2 + \left(\frac{u(f_{n0})}{f_{n0}}\right)^2} \\ &\approx \sqrt{\left(\frac{\varepsilon_d}{1+\varepsilon_d}\right)^2 E_{\varepsilon_d}^2 + E_{f_n}^2 + E_{f_{n0}}^2} \end{aligned} \tag{8}$$

and for the needle measurements $^{(ne)}$

$$\begin{aligned} E_{c_r}^{(ne)} &= \frac{u(c_r)}{c_r}^{(ne)} \\ &\approx \sqrt{\left(\frac{\Delta d}{d_0+\Delta d}\right)^2\left(\left(\frac{u(\Delta d)}{\Delta d}\right)^2 + \left(\frac{u(d_0)}{d_0}\right)^2\right) + \left(\left(\frac{u(f_n)}{f_n}\right)^2 + \left(\frac{u(f_{n0})}{f_{n0}}\right)^2\right)} \\ &\approx \sqrt{\left(\frac{\Delta d}{(d_0+\Delta d)^2}\right)^2\left(E_{\Delta d}^2 + E_{d_0}^2\right) + E_{f_n}^2 + E_{f_{n0}}^2} \end{aligned} \tag{9}$$

Table 2: Measurement uncertainty description

Variable x_i	Related to	Description
misc†	Sample	Based on thickness reduction of 5 samples. 3 ARAMIS + 2 Needle.
misc††	Sample	Based on variation in thickness reduction of sample A and B.
f_{n0}	Acoustics	Based on distribution of 50 acoustic shots at zero loading.
f_n	Acoustics	Based on distribution of groups of 50 consequtive acoustic shots.
Δf	Acoustics	Calculation of resonance frequency can be done to numeric precision.
ε_d	ARAMIS	Capability of ARAMIS hardware and software [26, 25]. Dependent on the resolution and distribution of the stochastic spray pattern.
$\varepsilon_{d\mathrm{std}}$	ARAMIS	Based on distribution of ARAMIS measurement values in the area of the acoustic footprint.
d_0	Needle	Based on micrometer screw measurements.
$d_{0\|\|}$	Needle	Related to initial parallellity of sample in the area of the acoustic footprint
Δd	Needle	Based on resolution of each needle.
$\Delta d_{\|\|}$	Needle	Related to variation in thickness development in the area of the acoustic footprint during loading

The total uncertainty can thus be expressed as

$$E_{tot} = \sqrt{E_{c_r}^2 + E_{misc}^2} \tag{10}$$

As can be seen from Eqs. (6) and (8) the uncertainty related to the initial thickness d_0 falls out of the uncertainty budget for the ARAMIS measurements. The uncertainty in ε_d consists of the measurement uncertainty and the variation in the measurements over the area where it has been calculated. In addition E_{ε_d} has a sensitivity coefficient of $\varepsilon_d/(1+\varepsilon-d)$ which varies between 0 and 0.065. The contribution from the ARAMIS measurement uncertainties is thus of the order of ∼0.006 %, while the contribution from variation over the acoustic footprint has been measured to be of the order of ∼1 %.

As the needle measurements have not been used in this paper, the related uncertainties are only included for reference. From Eq. (9) the sensitivity coefficient of both d_0 and Δd is $\Delta d/(d_0+\Delta d)$, and varies between 0 and 0.065. The contribution from the initial thickness measurements has been estimated to be of the order of ∼0.01 %, and is assumed to incorporate the variation in thickness over the acoustic footprint. The resolution of the needle measurements gives a contribution of ∼0.03 %. In addition the variation in thickness change over the acoustic footprint must be taken into account. It has been assumed that this is of the same order of magnitude as the variation measured by ARAMIS $\sim E_{\varepsilon_{d\mathrm{std}}}$.

The uncertainty of the acoustic measurements is related to signal excitation, propagation, response of target, signal capturing, electronic processing, and calculation of resonance frequencies. The calculation of the resonance frequencies can be done to numerical precision, and is thus negligible. The remaining uncertainties are all related to the actual acoustic measurement, and can be estimated by the variation of measured frequencies within a group of acoustic shots done under the same conditions. For each group of 50 acoustic shots the relative standard deviation of the measured resonance frequencies has been calculated. On average this uncertainty contribution is of the order of ∼0.01 %.

A summary of the uncertainties and the relative contributions to the total uncertainty is shown in Table 2 and 3. The last column in Table 3 "Uncertainty contribution" shows the standard relative uncertainty multiplied with the sensitivity coefficient.

4 Results and discussion

For the acoustic measurement of frequency response seven tests have been performed. The resonance frequencies with the largest excited energy were mainly the 2nd and 3rd TE harmonic at approximately

Table 3: Measurement uncertainties

	$\mu(x_i)$	$u(x_i)$	Distribution	Confidence level [%]	E_{xi} [%]	Sensitivity coeff.	Uncertainty contribution [%]
misc†	6.5 %	0.45 %	Normal	68	6.9	1.000	**6.9**
misc††	6.0 %	0.1 %	Rectangular	100	1.7	1.000	**1.7**
f_{n0}*	893 kHz	65 Hz	Normal	68	7.3e-3	1.000	**7.3e-3**
f_n*	893+δf kHz	$\sim$ 100 Hz	Normal	68	1.2e-2	1.000	**1.2e-2**
Δf	893+δf kHz	$\sim$ 1 Hz	Rectangular	100	6.3e-5	1.000	**6.3e-5**
ε_d	0-6 %	$\sim$ 0.01 %	Rectangular	100	9.6e-2	0.064	**6.1e-3**
$\varepsilon_{d\mathrm{std}}$	0-6 %	$\sim$ 1 %	Normal	68	17	0.064	**1.1**
d_0	9.95 mm	0.024 mm	Normal	68	0.2	0.064	**1.6e-2**
$d_{0\|\|}$**	-	-	Normal	68	-	0.064	-
Δd	0-0.6 mm	0.002 mm	Rectangular	100	0.3	0.064	**3.0e-2**
$\Delta d_{\|\|}$***	-	-	Normal	68	-	0.064	-

* For the 893 kHz resonance a linear relation between the applied strain and the measured resonance frequency within each group of 50 shots has been observed. This indicates that the uncertainty in the measured resonance frequencies were less than the normal distribution applied in the current uncertainty analysis.
** Assumed to be incorporated in E_{d_0}
*** Not evaluated, but assumed to be of an order of magnitude comparable to $E_{\varepsilon_{d\mathrm{std}}}$

600 kHz and 900 kHz, and the 3rd TS harmonic at approximately 495 kHz. Because of noise the test data for the 495 and 600 kHz resonances had a higher variation than the 900 kHz data. This paper has thus focused on the 3rd TE harmonic measured to be at 893 kHz for the unloaded specimen which gives the most consistent acoustic measurements.

Because of the large uncertainty related to the thickness development of the specimens, two specimens (A and B) have been selected based on the best match of the dimensions of the undeformed and deformed thickness and cross section at the U-notch. The acoustic results from specimen (specimen A) have been combined with the thickness measurement of (specimen B). Assuming a rectangular distribution of the difference in thickness development between the two specimens, the E_{misc} is reduced to $\sim$2 %. The contribution from the *misc* uncertainty will be investigated and reduced in future work. From these results the sound velocity change has been calculated as a function of measured strain. The applied stress-strain history of the tests are shown in Fig. 4 where the applied normalised engineering stress (tension force in x-direction divided by the initial cross section at the notch normalised to the yield limit) is plotted on the y-axis while the measured strain in x-direction is plotted on the x-axis. Points of the load history have been enumerated with capital letters. The displacement controlled loading sequences is illustrated by the line segments AC, DE, FG, and HI, while the force controlled unloading is illustrated by the line segments CD, EF, GH, and IJ. The first line segment AB represent the initial elastic deformation, while deformation beyond point B is plastic. During unloading and loading of each of the line segments (CE, EF, GH, and IJ) the specimens behave elastically. In addition the average normalised stress and strain for specimen A is plotted for each group of 50 measurements including two standard deviations in applied normalised stress and measured strain. The errorbars may for some groups be so small that they do not show in the figure. For each of the acoustic shots on specimen A, the 3rd TE harmonic frequency has been measured and combined with the corresponding ARAMIS thickness measurement of specimen B. The mean value and corresponding relative uncertainty (at 95 % confidence) over 50 acoustic shots for relative frequency and thickness changes are shown in Figs. 5a and 6a, respectively, as a function of measured strain. Figs. 5b and 6b shows the deviation in Figs. 5a and 6a from a linear behaviour (dashed line) between the first and last measurements.

Fig. 5a and 6a shows that the relative change in frequency and thickness are of similar magnitude (maximum measured relative frequency and thickness change were 6.13 % and -6.82 %, respectively). This implies that most of the measured frequency change corresponds to a change in thickness during loading, and only small variations can be linked to the change of sound velocity.

Based on the measured frequency and corresponding thickness the sound velocity was calculated

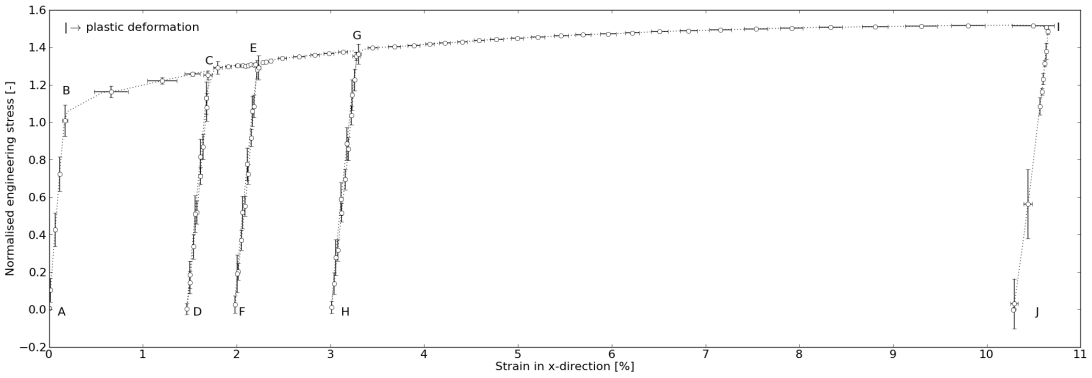

Figure 4: Stress - strain history with mean value and two standard deviations for groups of 50 acoustic shots.

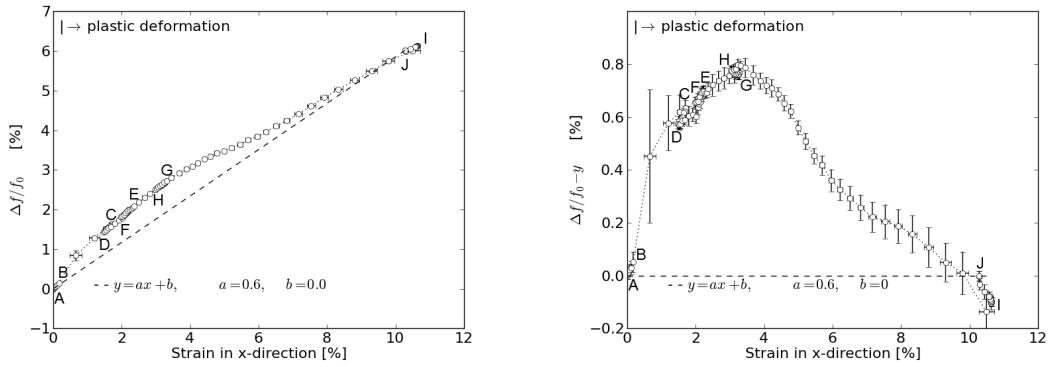

(a) Frequency change

(b) Deviation from linear frequency change

Figure 5: Relative frequency change for the 3rd TE harmonic (initially at 893kHz) during loading for specimen A. Uncertainties are plotted at 95 % confidence

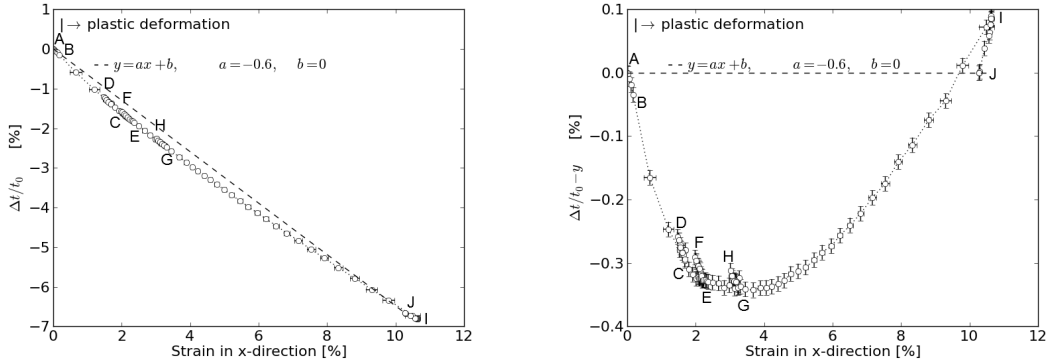

(a) Thickness change

(b) Deviation from linear thickness change

Figure 6: Relative thickness change during loading for specimen B, excluding $E_{\varepsilon_d \mathrm{std}}$. Uncertainties are plotted at 95 % confidence.

according to Eq. (1) with the standard relative uncertainty of Eq. (8), excluding $E_{misc\dagger\dagger}$ and $E_{\varepsilon_d \mathrm{std}}$. Fig. 7 shows the calculated relative sound velocity change as a function of applied strain. The maximum positive relative sound velocity change of approximately 0.25 % was measured around 1.0 % strain,

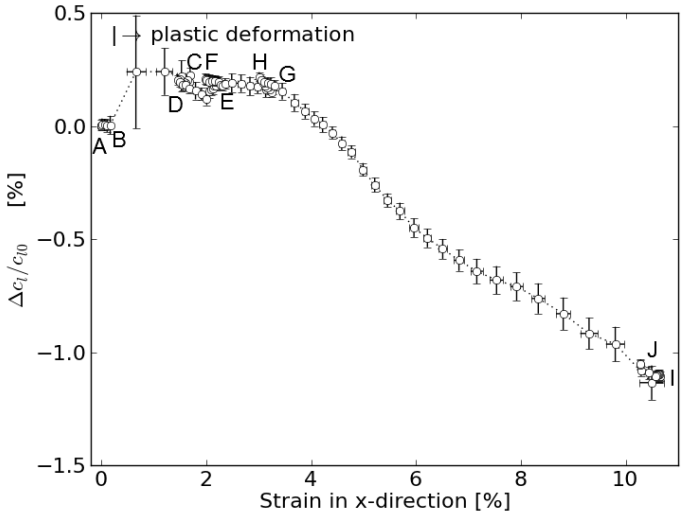

Figure 7: Relative sound velocity change during loading for 3rd TE harmonic (initially at 893kHz). The preliminary uncertainties $E_{\varepsilon_d \mathrm{std}}$ and $E_{misc\dagger\dagger}$ are not included. The other uncertainties are plotted at 95 % confidence.

at onset of plastic deformation (Fig. 4). After this the sound velocity decreases to the maximum negative relative sound velocity change of approximately 1.1 % at 10.5 % strain (at maximum test load). The largest change in relative sound velocity occurs at onset of plastic deformation (region BC). This region of the loading history has a larger deformation rate than any other region, and accordingly the measurements have a larger variation in measured resonance frequency and corresponding thickness and applied strain. This also leads to larger error bars in this region for Figs. 4 - 7. Here the change in relative sound velocity is of the order of ∼0.25 % betwen two groups of measurements, which is one order of magnitude larger than for any other regions. In the elastic regions the measured change in relative sound velocity was in the order of 0.01 % over 0.2-0.3 % strain (region AB, CD, EF, GH, and IJ). These values have been based on the measured values ignoring the measurement uncertainties.

As can be seen from Table 3 and Eq. (10), the preliminary uncertainties $E_{misc\dagger\dagger}$ and $E_{\varepsilon_d \mathrm{std}}$ dominate with a relative uncertainty contribution of 1.7 % and 1.1 %, respectively. The other uncertainties contribute less than ∼0.1 % (Fig. 7). This indicates that although the development of relative change in sound velocity with increasing strain progressed in a manner which was anticipated, the quantity of change could not be determined accurately from use of the two test specimens A and B, as presented in this paper. However, the methodology can be used to test a large number of specimens with close to matching material properties and geometry to make a statistical distribution of the relationship between the applied stress and calculated sound velocity. Hopefully this procedure may contribute to reduce the $E_{misc\dagger\dagger}$ uncertainty contribution significantly. Preliminary tests of straight specimens have been performed, which shows that the uncertainty contribution from variation over the acoustic footprint can be reduced with one order of magnitude for specimens with a more homogeneous stress distribution. Future experiments will consider the use of straight specimens, or an extended waist, instead of the current U-notch.

From Fig. 4 the five elastic loading/unloading sequences (AB, CD, EF, GH, and IJ) can clearly be seen around 0, 1.5 %, 2.0 %, 3.0 %, and 10.3 % strain. In these regions the test specimen behaves elastically, and the effect on the thickness and frequency measurements can be seen in Fig. 8 which shows a zoom of Figs. 5b, 6b and 7. Both the frequency, thickness, and resulting sound velocity change indicate that the behaviour in each of the elastic regions is similar and of the same order of magnitude, while substantially different from the behaviour during plastic deformation. The current measurements have not been sufficiently focused on the behaviour in the elastic region to be able to draw any conclusion on how well the described measurement methodology is able to capture the slight sound velocity change

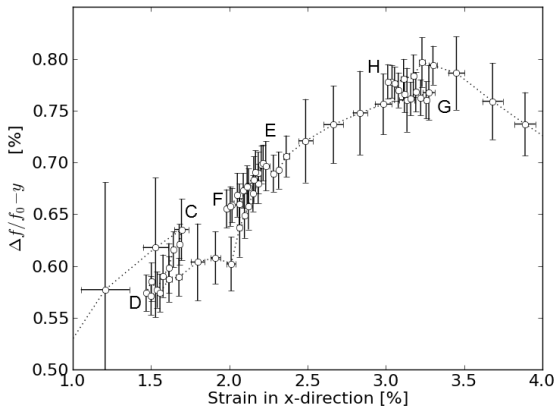

(a) Relative frequency change

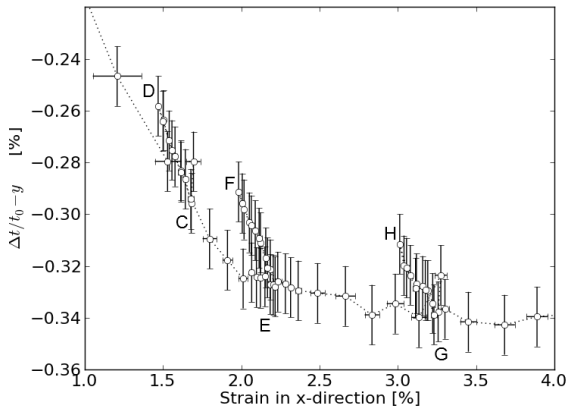

(b) Relative thickness change

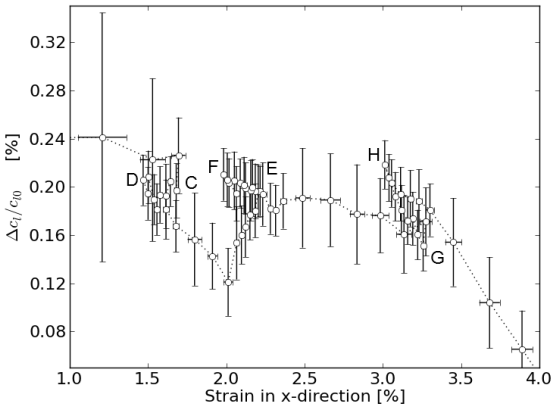

(c) Relative sound velocity change

Figure 8: Zoom of Figs. 5b, 6b, and 7, to focus on the regions of elastic unloading/loading, at 1.5 %, 2 %, and 3 % strain

in the elastic region (one to two orders of magnitude less than the sound velocity change owing to plastic deformation). This will be investigated in future work.

As mentioned above the large deformation rate in region BC at onset of plastic deformation leads to fewer measurements in this region. Since this region also shows a significant jump in relative sound velocity change (Fig. 7) it is important to investigate this further in future work.

It should also be noted that the sound velocity is dependent on the temperature [28]. The presented results have all been done at ambient room temperature, and it has been assumed that the temerature has not varied during the tests (i.e. negligible effect on the sound velocity). Possible effects of temperature influence is planned to be investigated in future work.

5 Conclusion

In this paper a methodology to measure changes in the compressional sound velocity of steel owing to the acousto-elastic/plastic effects using the Acoustic Resonance Technology has been investigated.

As can be seen from Fig. 7, the measured change in velocity is quite small (in the order of a few tenths of a percent) for a large plastic deformation, and even smaller in the elastic regime. These results

are based on the measured change in resonance frequency and the measured change in thickness of the specimen, which are of the same order of magnitude. To be able to conclude on the significance of the measured sound velocity changes it would be preferred that both measurements were done accurately on the same test specimen. Since this has not been possible with the current setup, a large number of resonance and thickness measurements should be combined to develop a statistical distribution of the sound velocity dependency. This approach will be investigated in future work.

6 Acknowledgements

This work is part of a PhD study of the first authour performed in collaboration between Det Norske Veritas and The University of Bergen, Norway. The work is financed by Gassco and The Research Council of Norway

References

[1] P. Withers and H. Bhadeshia, "Residual stress. part 1 - measurement techniques," *Materials Science and Technology*, vol. 17, pp. 355–365, Apr. 2001.

[2] P. Withers and H. Bhadeshia, "Residual stress. part 2 - nature and origins," *Materials Science and Technology*, vol. 17, pp. 366–375, Apr. 2001.

[3] F. A. Kandil, J. D. Lord, A. T. Fry, and P. V. Grant, "A review of residual stress measurement methods - a guide to technique selection," tech. rep., Queens Road, Teddington, Middelsex, TW11 0LW, UK, 2001.

[4] F. D. Murnaghan, *Finite deformation of an elastic solid.* New York: Wiley, 1951.

[5] D. S. Hughes and J. L. Kelly, "Second-Order elastic deformation of solids," *Physical Review*, vol. 92, p. 1145, Dec. 1953.

[6] R. H. Bergman and R. A. Shahbender, "Effect of statically applied stresses on the velocity of propagation of ultrasonic waves," *Journal of Applied Physics*, vol. 29, no. 12, p. 1736, 1958.

[7] J. Frankel, W. Scholz, G. Capsimalis, and W. Korman, "Residual stress measurement in circular steel cylinders," in *Ultrasonics Symposium Proceedings* (B. R. McAvoy, ed.), (Atlanta, Georgia), pp. 1009–1012, Oct. 31 – Nov. 2 1983.

[8] A. A. Chernoochenko, F. G. Makhort, and O. I. Gushcha, "Use of the theory of acoustoelasticity of rayleigh waves to determine stresses in solids," *International Applied Mechanics*, vol. 27, pp. 38–42, Jan. 1991.

[9] J. Kyung-Young, Q. Hai-Hua, H. Job, and K. Noh-Yu, "Estimation of clamping force in high-tension bolts through ultrasonic velocity measurement," *Ultrasonics*, vol. 44, pp. e1339–e1342, Dec. 2006.

[10] S. D. V. V. Mishakin and M. D. G. Potter, "The use of wide band ultrasonic signals to estimate the stress condition of materials," *Journal of Physics D: Applied Physics*, vol. 39, no. 21, pp. 4681–4687, 2006.

[11] M. Kobayashi, "Ultrasonic nondestructive evaluation of microstructural changes of solid materials under plastic deformation - Part II. Experiment and simulation," *International Journal of Plasticity*, vol. 14, no. 6, pp. 523–535, 1998.

[12] E. Schneider, "Evaluation of stress states of components using ultrasonic and micro magnetic techniques," in *ASME Conference Proceedings*, vol. 2009, (Prague, Czech Republic), pp. 231–239, ASME, 2009.

[13] D. Roylance, "Yield and plastic flow." http://ocw.mit.edu/courses/materials-science-and-engineering/3-11-mechanics-of-materials-fall-1999/modules/yield.pdf, October 2001, last viewed 2012-03-27.

[14] M. Kobayashi, "Ultrasonic nondestructive evaluation of microstructural changes of solid materials under plastic deformation - Part I. Theory," *International Journal of Plasticity*, vol. 14, no. 6, pp. 511–522, 1998.

[15] M. Kobayashi, S. Tang, S. Miura, K. Iwabuchi, S. Oomori, and H. Fujiki, "Ultrasonic nondestructive material evaluation method and study on texture and cross slip effects under simple and pure shear states," *International Journal of Plasticity*, vol. 19, pp. 771–804, June 2003.

[16] L. B. Zuev, B. S. Semukhov, and K. I. Bushmeleva, "Dependence of the ultrasound velocity on the acting stress during plastic flow of polycrystals," *Technical Physics*, vol. 44, pp. 1489–1490, Dec. 1999.

[17] L. B. Zuev, V. I. Danilov, S. A. Barannikova, and V. V. Gorbatenko, "Autowave model of localized plastic flow of solids," *Physics of Wave Phenomena*, vol. 17, pp. 66–75, Feb. 2009.

[18] M. Kobayashi, "Analysis of deformation localization based on proposed theory of ultrasonic wave velocity propagating in plastically deformed solids," *International Journal of Plasticity*, vol. 26, pp. 107–125, Jan. 2010.

[19] G. Maze, J. L. Izbicki, J. Ripoche, A. Nagl, H. Uberall, and K. B. Yoo, "Transient acoustic scattering from layers and plates," *The Journal of the Acoustical Society of America*, vol. 80, pp. 295–301, July 1986.

[20] C. C. H. Guyott and P. Cawley, "The measurement of through thickness plate vibration using a pulsed ultrasonic transducer," *The Journal of the Acoustical Society of America*, vol. 83, pp. 623–631, Feb. 1988.

[21] N. Stål, "Norsk stål - produkt katalog." http://www2.norskstaal.no/varekatalog/, Last viewed 2012-03-29.

[22] PCT, "Pct homepage." http://www.pct-ltd.co.uk/, Last viewed 2012-03-29.

[23] Instron, "Instron homepage." http://www.instron.se/, Last viewed 2012-03-29.

[24] MessTek, "Messtek homepage." http://messtek.com/, Last viewed 2012-03-29.

[25] GOM mbH, Mittelweg 7-8, D-38106 Braunschweig, Germany, *ARAMIS User Manual - Software, Rev. aramis-v6-3_1st_en_rev-a*, May 2011.

[26] GOM mbH, Mittelweg 7-8, D-38106 Braunschweig, Germany, *ARAMIS User Information - Hardware, Rev. aramis_hw-2lt-4-5-5lt-12-hs-adjustable_en_rev-a*, May 2011.

[27] G. mbH, "Aramis homepage." http://www.gom.com/metrology-systems/system-overview/aramis.html, Last viewed 2012-03-29.

[28] T. Rommetveit, *Development of Non-invasive Ultrasound Inspection Techniques through Steel*. PhD thesis, Norwegian University of Technology, Trondheim, Norway, 2011.